Ultrasonics 53 (2013) 53–64

Contents lists available at SciVerse ScienceDirect

Ultrasonics

journal homepage: www.elsevier.com/locate/ultras

Quantitative assessment of effects of phase aberration and noise on high-frame-rate imaging

Hong Chen, Jian-yu Lu *

Ultrasound Laboratory, Department of Bioengineering, University of Toledo, Toledo, OH 43606, United States

ARTICLE INFO

Article history:
Received 13 January 2012
Received in revised form 22 March 2012
Accepted 27 March 2012
Available online 5 April 2012

Keywords:
Delay-and-sum
High-frame-rate
Phase aberration
Sidelobe ratio
Energy ratio

ABSTRACT

The goal of this paper is to quantitatively study effects of phase aberration and noise on high-frame-rate (HFR) imaging using a set of traditional and new parameters. These parameters include the traditional −6-dB lateral resolution, and new parameters called the energy ratio (ER) and the sidelobe ratio (SR). ER is the ratio between the total energy of sidelobe and the total energy of mainlobe of a point spread function (PSF) of an imaging system. SR is the ratio between the peak value of the sidelobe and the peak value of the mainlobe of the PSF. In the paper, both simulation and experiment are conducted for a quantitative assessment and comparison of the effects of phase aberration and noise on the HFR and the conventional delay-and-sum (D&S) imaging methods with the set of parameters. In the HFR imaging method, steered plane waves (SPWs) and limited-diffraction beams (LDBs) are used in transmission, and received signals are processed with the Fast Fourier Transform to reconstruct images. In the D&S imaging method, beams focused at a fixed depth are used in transmission and dynamically focused beams are used in reception for image reconstruction.

The simulation results show that the average differences between the −6-dB lateral beam widths of the HFR imaging and the D&S imaging methods are −0.1337 mm for SPW and −0.1481 mm for LDB, which means that the HFR imaging method has a higher lateral image resolution than the D&S imaging method since the values are negative. In experiments, the average differences are also negative, i.e., −0.2804 mm for SPW and −0.3365 mm for LDB. The results for the changes of ER and SR between the HFR and the D&S imaging methods have negative values, too. After introducing phase aberration and noise, both simulations and experiments show that the HFR imaging method has also less change in the −6-dB lateral resolution, ER, and SR as compared to the conventional D&S imaging method. This means that the HFR imaging method is less sensitive to the phase aberration and noise.

Based on the study of the new parameters on the HFR and the D&S imaging methods, it is expected that the new parameters can also be applied to assess quality of other imaging methods.

1. Introduction

High-frame-rate (HFR) ultrasound imaging method with one transmission wave to reconstruct images in Fourier domain was proposed by Lu in 1997 [1] and verified experimentally in 1998 [2]. This method transforms a slice of radio-frequency (RF) echo signals from time domain into temporal Fourier domain, and then the signals are mapped from the temporal Fourier domain into a spatial Fourier domain to reconstruct B-mode images by the inverse Fourier transform. Image frame rate of the HFR imaging method with one transmission can be up to 3750 frames/s for imaging biological soft tissue at a depth of 200 mm [1]. In 2006, the HFR imaging method was extended to cover a large field of view, such as 90°, using multiple transmissions, such as 91 transmissions [3]. In this method, instead of reconstructing an image from multiple A-lines, the image is reconstructed by a coherent superposition of multiple slices of reconstructed images. It is worth noting that although the HFR imaging method is promising for clinical use, commercialization of this technology may require a fundamental change to the traditional D&S beamforming architecture that has dominated the market over the past few decades and will need a large capital investment. Unless it is significantly profitable, commercial companies may be reluctant to make such a transition away from the D&S beamforming architecture. However, as the technologies such as microelectronics advance and thus the power consumption and costs of electronics are lowered, the HFR imaging method will be more attractive to commercial vendors. Due to the significance of the HFR imaging method to future ultrasound imaging technology, it is necessary to quantitatively study the effects of phase aberration and noise on the HFR imaging method.

* Corresponding author.
E-mail addresses: chenhong44@gmail.com (H. Chen), jilu@eng.utoledo.edu (J.-y. Lu).

0041-624X/$ - see front matter
http://dx.doi.org/10.1016/j.ultras.2012.03.013

Human tissues have inhomogeneous speed of sound, which causes phase aberration to ultrasound beams and thus distorts images. Electrical noise of ultrasound imaging systems cannot be completely removed and thus it degrades image quality. Although some studies on the effects of phase aberration and noise have been conducted previously on the HFR and the D&S imaging methods, they are limited. For example, in 2000 [4,5], investigations that only studied experimentally the effects of phase aberration on grayscale objects and studied qualitatively the effects of noise on a point target with a computer simulation were conducted to compare the effects of phase aberration and noise on the HFR and the D&S imaging methods that are produced with a single plane wave transmission. In 2007 [6], the effects of phase aberration and noise on the extended HFR imaging method were qualitatively studied with an experiment on the contrast of a cystic target of an ATS539 tissue-mimicking phantom at a specific depth near the center of reconstructed images and compared with the D&S imaging method. Although cystic targets are traditionally used to assess image contrast, there is no standard procedure for a quantitative assessment with these targets. For example, it is difficult to select the size of the cyst, the area inside the cyst, and background area in an image. Since biological soft tissues can be modeled as a superposition of multiple single point scatterers and each point scatterer can be easily defined, it is beneficial to establish some parameters for the point scatterer to assess image quality such as resolution and sidelobes in addition to using the method with cystic targets.

The −6-dB image resolution has long been established for assessing the quality of images of a point scatterer [1,6] and is calculated based on the point spread function (PSF) of the images. Although this parameter provides part of the quantitative information of the image quality, it does not include sidelobe information of the image, which affects the image contrast. To quantitatively study the sidelobes of images using point scatterers, in this paper, new parameters based on the PSF of the images will be proposed and used together with the −6-dB lateral resolution to study the effects of phase aberration and noise on the HFR and the D&S imaging methods. The new parameters will be complementary to traditional ones for a quantitative assessment of the quality of reconstructed images and will be useful in providing information for the correction of phase aberration.

In this paper, detailed explanation on the newly proposed set of parameters that are used to assess the quality of ultrasound B-mode images will be given in Section 2. A process to add phase aberration and noise into simulated and experimentally obtained images will also be given in this section. Simulation of an object containing a total of 8 point scatterers in axial and lateral directions and its results are given in Section 3. Conditions for *In-vitro* experiments based on a modified AIUM 100-mm standard test object and the experiment results will be given in Section 4. In Sections 5 and 6, we will have a discussion and a conclusion respectively.

2. Parameters and conditions

2.1. Parameters for assessing quality of images

Instead of assessing image quality qualitatively by the human eyes, a set of parameters is proposed in this paper to quantitatively measure the image quality for the effects of phase aberration and noise on the HFR and the D&S imaging methods. The set of parameters include the −6-dB lateral resolution, the ratio of sidelobe energy to mainlobe energy (energy ratio or short for ER), and the ratio of maximum sidelobe peak value to mainlobe peak value (sidelobe ratio or short for SR). It is important to know that the proposed set of parameters is focused on the point spread function (PSF) of imaging methods since a quantitative analysis of image contrast based on images of a cyst target of an ATS 539 tissue-mimicking phantom has already been studied [5]. Moreover, only the maximum envelope of the PSF along the lateral direction is studied because the −6 dB resolution, ER, and SR along axial direction depends mainly on the bandwidth of the transducer used. A detailed explanation of the −6-dB lateral resolution, ER, and SR is given below.

Resolution of an image is defined as the minimum distance between which two point scatterers can be distinguished in the image. Therefore, resolution is an important parameter to assess image quality. In this paper, the −6 dB lateral beam width of the maximum envelope of the PSF of the imaging methods will be used as one of the parameters to quantitatively measure the quality of ultrasound images. The −6 dB lateral beam width is defined as the lateral distance between two points whose values are half of that of the peak of the mainlobe in a plot of the maximum envelope of the PSF over the lateral direction (see Fig. 1c). It is worth noting that a smaller −6-dB lateral beam width corresponds to a higher lateral image resolution or a high image quality, i.e., the lateral image resolution is inversely proportional to the lateral beam width.

Sidelobe is produced by edge waves of transducers and appears on both sides of the mainlobe. It produces artifacts in ultrasound images and lowers image contrasts. Therefore, it is necessary to characterize the sidelobe for assessing image quality. The second parameter used for image quality analysis is the energy ratio or ER, which describes the energy distribution of the maximum envelope of the PSF between the areas under the sidelobe and the mainlobe. The formula for calculating the ER is given in Eq. (1), where $value\_PSF_i$ is the value of the maximum envelope of the PSF at the ith lateral position. A lower ER value means a higher image quality since sound energy is more concentrated in the mainlobe of the image of a point scatterer than in the sidelobe areas.

$$\mathrm{ER} = \left(\sum_{i}^{sidelobe\_area} (value\_PSF_i)^2 \right) \Bigg/ \left(\sum_{j}^{mainlobe\_area} (value\_PSF_j)^2 \right) \qquad (1)$$

As shown in Fig. 1c, the lateral positions of the boundaries of the mainlobe area is determined by the intersections of the lines that are extended from the peak of the mainlobe through the −10 dB points of the mainlobe peak on both sides of the mainlobe. The sidelobe areas are defined as all areas that are not in the mainlobe. Apparently, ER will increase in ultrasound imaging when there is phase aberration [7] that may cause a split of the mainlobe, resulting in a shrunk mainlobe area and an expanded sidelobe area.

The third parameter that is used for the assessment of image quality is the sidelobe ratio or SR. This parameter is calculated with Eq. (2) where *sidelobe_peak* and *mainlobe_peak* are the peak values of the sidelobe and mainlobe, respectively, in the plot of the maximum envelope of the PSF (see Fig. 1c). Image quality is degraded when SR becomes larger after phase aberration or noise is introduced during an imaging process.

$$\mathrm{SR} = sidelobe\_peak/mainlobe\_peak \qquad (2)$$

Although the plot of the maximum envelope of the PSF over the lateral distance (see Fig. 1c) has been used to show both the mainlobe and sidelobes, as in the study of effects of motion on a simulated PSF of the HFR imaging method in [8], it is not quantitative. Large sidelobes can produce artificial objects in reconstructed images. SR provides a convenient quantitative single-parameter assessment on the size of the maximum sidelobe relative to the mainlobe.

The three parameters, i.e., the −6-dB lateral resolution, ER, and SR provide complementary information on image quality. A high −6-dB lateral resolution indicates a sharper image, a high ER represents images of low contrast, and a high SR means that a single

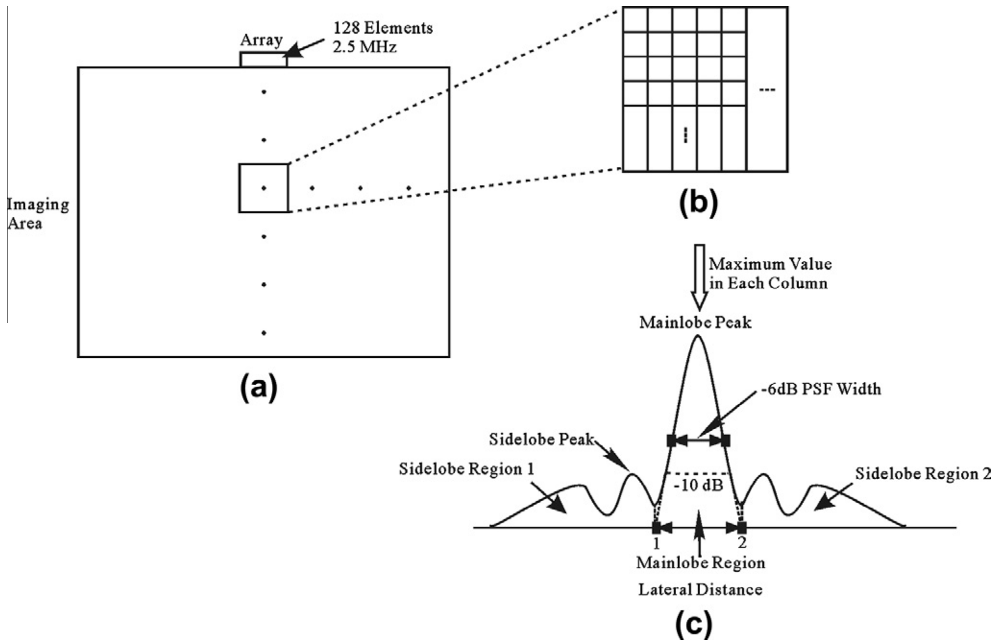

Fig. 1. Procedures for obtaining a maximum envelope plot of the point spread function (PSF) of a B-mode image of a point scatterer. An imaging area that contains 9 point scatterers is shown in (a). A magnified area that is cropped from the B-mode image is shown in (b). A plot of the maximum envelope of the PSF over the lateral distance is in (c). The vertical value of the plot is the maximum value of a column of the cropped image. The −6-dB lateral resolution, mainlobe, sidelobes, and the areas under the mainlobe and sidelobes are illustrated in the plot. The boundaries ("1" and "2") between the mainlobe and the sidelobes are determined by the intersections of the lines that are extended from the peak of the mainlobe through the −10-dB points of the mainlobe with the lateral axis.

point scatter may appear split in the image. In short, the three parameters need to be used altogether to fully characterize effects of phase aberration and noise on the HFR imaging method.

2.2. Addition of phase aberration and noise

Phase aberration is caused by a local variation of speed of sound in different human tissues [7]. The most common source of phase aberration in ultrasound imaging is the fat layer that is close to the ultrasound transducer, as described in [6]. Phase aberration affects both ultrasound transmission and reception in the imaging process. In this paper, phase aberration is added into the imaging process in both transmission and reception using a phase screen model. The phase screen will cause a peak-to-peak change of the phase of $3\pi/2$ (or 0.75 wavelengths) as shown in Fig. 2. This phase screen is selected from one of the two phase screens used in [5,6] for an easier comparison of the results of this study with previous studies. A flow chart for the addition of phase aberration in both transmission and reception in imaging is shown in Fig. 3a.

Random noise is also a factor in reducing ultrasound image quality. The noise is mainly from the electrical noise of an imaging

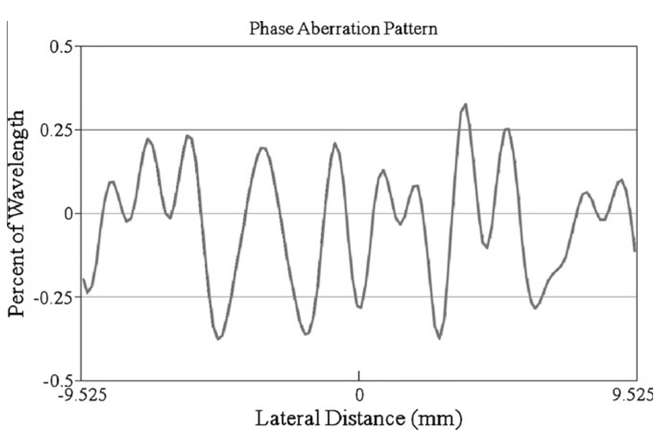

Fig. 2. A phase screen that is used to introduce phase aberration. The range of the phase shift of the phase screen is from $-3\pi/4$ to $3\pi/4$ ($-3/8$ to $3/8$ wavelengths), giving a peak-to-peak phase shift of $3\pi/2$ (3/4 wavelengths). The center ultrasound wavelength used for the phase screen in both the simulation and the experiment is 0.6 mm.

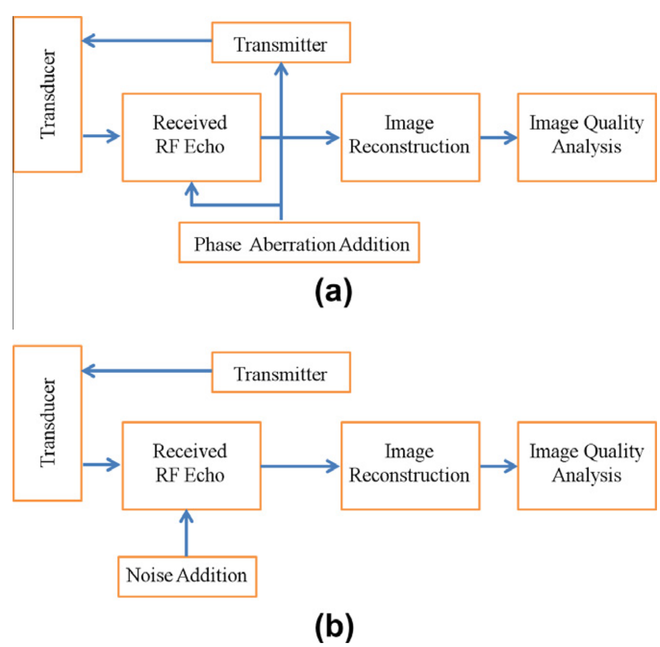

Fig. 3. Flow charts for introducing (a) the phase aberration and (b) the noise into the high-frame-rate (HFR) and the delay-and-sum (D&S) imaging methods. The phase aberration is added to both transmission and reception and the noise is added only to the received radio-frequency (RF) echo signals.

system. In this paper, pseudo random noise pattern is used so that the same pattern can be used in both simulation and experimental studies. The noise bandwidth is equal to the two-way bandwidth of the one-dimensional (1D) array transducer used in the experiments, i.e., 58% of transducer center frequency. To achieve such a noise bandwidth, a two-way Blackman window function is used to filter the pseudo-random noise in the frequency domain. The maximum amplitude of the noise was set to be 50% of that of the entire echo data set (global maximum), which gives a signal-to-noise ratio of 6 dB. The addition of the noise is shown in the flow chart in Fig. 3b.

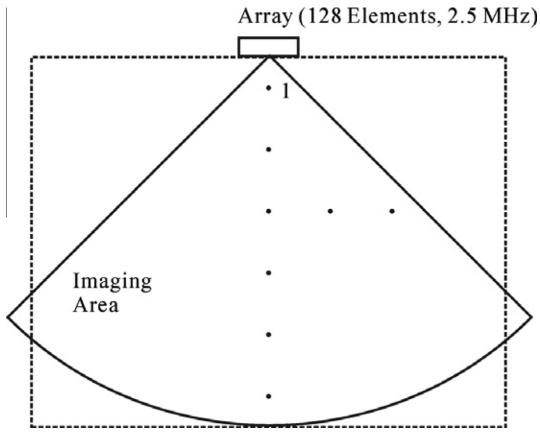

Fig. 4. Imaging area that includes 8 point scatterers in the simulation study. Six point scatterers are located at depths of 10, 30, 50, 70, 90, 110 mm, respectively, and 2 point scatterers are located on lateral positions of 20 and 40 mm, respectively, at a depth of 50 mm. The area of the final B-mode image, indicated by the dashed frame, has a width of 153.6 mm and a depth of 120 mm.

3. Simulation and results

3.1. Simulation conditions

In the simulation study, a total of 8 point scatterers are assumed in the imaging area (see Fig. 4). Six point scatterers are located at depths of 10, 30, 50, 70, 90, 110 mm, respectively, along the axial axis of the transducer, and 2 point scatterers are located at a depth of 50 mm and at lateral positions of 20 and 40 mm, respectively. Such an arrangement of point scatterers allows us to study the effects of phase aberration and noise on the quality of images at depths ranging from 10 to 110 mm and lateral positions ranging from 0 to 40 mm, covering most of the imaging area.

In addition, the speed of sound is assumed to be 1450 m/s that is the same as that of the ATS539 tissue-mimicking phantom used in previous studies [5]. A one-dimensional (1D) phased array transducer with a center frequency of 2.5 MHz, 128 elements (19.2 mm $\times$ 14 mm aperture size), and about a 58% -6-dB two-way fractional bandwidth that is obtained by squaring the Blackman window function is also assumed (notice that the

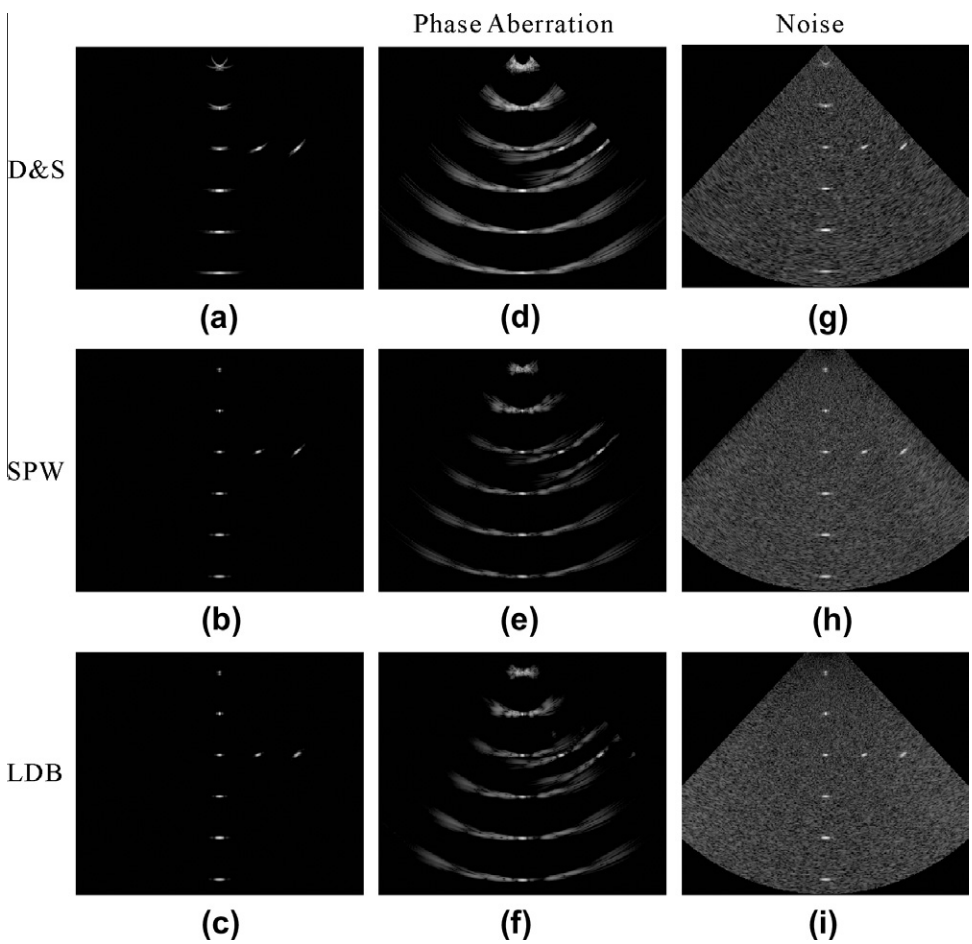

Fig. 5. Images reconstructed by the D&S (first row), steered plane wave (SPW) HFR (middle row), and limited-diffraction beam (LDB) HFR (bottom row) imaging methods from simulated echo data before adding a two-way phase aberration and the noise (left column), after adding the two-way phase aberration (middle column), and after adding the pseudo-random noise (right column). All images are log compressed at 50 dB to show details.

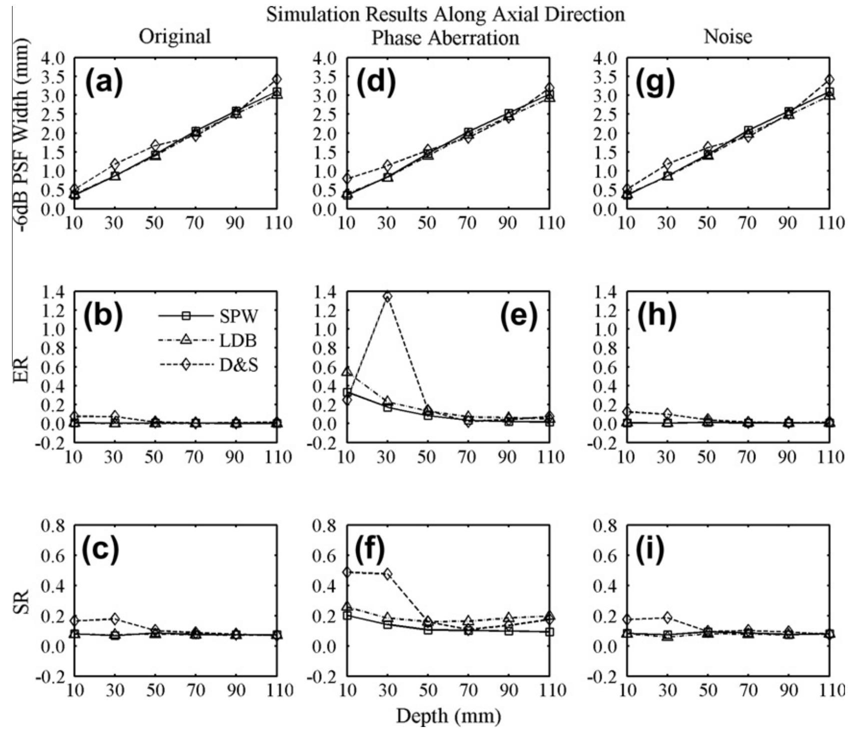

Fig. 6. Results of the −6 dB beam width (1st row), ER (2nd row), and SR (3rd row) of the simulated images of point scatterers in Fig. 5 along the axial direction for the D&S and the HFR imaging methods. The depths are at 10, 30, 50, 70, 90, and 110 mm. Panels (a–c) in the left column show the results for the −6 dB lateral beam width, ER, and SR, respectively, of images before adding the phase aberration and the noise. Panels (d–f) in the middle column show the results after adding the phase aberration. Results in Panels (g–i) are those after adding the noise. All panels in the figure contain three curves representing the results from the D&S, SPW, and the LDB imaging methods, respectively.

Table 1
Differences of −6 dB lateral beam widths between the HFR and the D&S imaging methods for the simulated images before adding the phase aberration and the noise. Results based on Fig. 6a for point scatterers along the axial direction at depths of 10, 30, 50, 70, 90, and 110 mm are shown in Panel (a), and results based on Fig. 8a for point scatterers along the lateral direction at lateral distances of 0, 20, and 40 mm at a depth of 50 mm are shown in Panel (b). SPW and LDB denote the HFR imaging methods with steered plane wave and limited-diffraction-beam transmissions, respectively.

	10	30	50	70	90	110
(a)						
SPW	−0.1550	−0.3080	−0.2375	0.1315	0.0477	−0.3209
LDB	−0.1327	−0.3180	−0.2760	0.0742	−0.0299	−0.4090

	0	20	40
(b)			
SPW	−0.2375	−0.0994	−0.0244
LDB	−0.2760	−0.1352	0.1701

electromechanical transfer function of a real ultrasound transducer can be approximated with a Blackman window function [9]). The parameters of the transducer are similar to those of a commercial Acuson V2 probe (Acuson, Mountain View, California, USA). The Acuson V2 probe was selected because it was available in our lab and had proper electrical connections and calibrations with our existing home-made imaging system [10,11]. This probe has also been used in the previous studies [6] and thus our results can be more easily compared.

The imaging area is of a sector shape (see Fig. 4) and has a field of view of 90° consisting of 91 transmissions that are steered beams focused at a fixed depth of 70 mm (for the D&S imaging), steered plane waves (for the HFR imaging), or limited-diffraction beams (for the HFR imaging). This focal depth is chosen so that the transmit beam is focused around the middle section of the images for an optimum imaging quality when using a single focus in the D&S imaging method. Images reconstructed have a size of 153.6 mm and 120 mm in the lateral and axial directions respectively as they are shown in the rectangle in Fig. 4 to include all point scatterers.

The simulation conditions above are chosen to be as close as possible to those of the experiment for comparison.

3.2. Simulation results

Images before adding the phase aberration and the noise for the D&S, steered plane wave (SPW), and limited-diffraction-beam (LDB) imaging methods are shown in Fig. 5a–c, respectively. Images after adding the phase aberration are given in Fig. 5d–f, and images with the noise added are in Fig. 5g–i. After adding the phase aberration, the sidelobes around the point scatterers are increased. The noise added fills out the otherwise clear background.

The −6-dB lateral resolution, ER, and SR are used to quantitatively assess image quality for all images in Fig. 5. Because the lateral distance between two neighboring point scatterers is 20 mm (see Fig. 4), the area for getting the maximum envelope of the PSF (see Fig. 1a) is set to be 20 mm by 20 mm to avoid influences from neighboring point scatterers. Parameters for assessing the image quality are calculated for scatterers arranged in both the lateral and axial directions (see Fig. 4).

3.2.1. Simulation results for point scatterers along axial direction

The simulation results for point scatterers along the axial direction are given in Fig. 6. The −6-dB lateral beam width (a smaller beam width means a higher resolution) of the images increases with the depth (see Figs. 6a, d, and g). To show the beam width relative to that of the D&S imaging method, the differences are

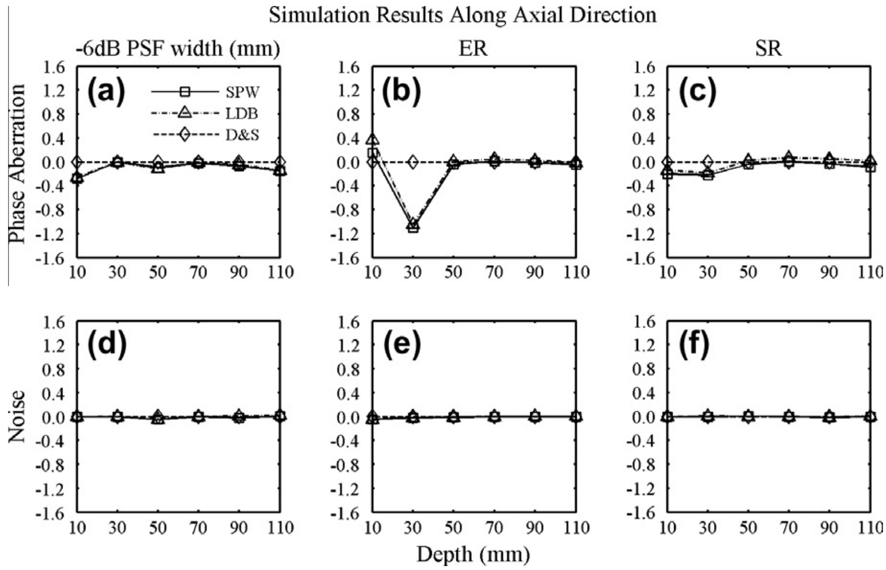

Fig. 7. Relative changes of the absolute changes of the −6-dB lateral beam width (Panels (a and d)), ER (Panels (b and e)), and SR (Panels (c and f)) after adding the phase aberration (1st row) and the noise (2nd row) at depths ranging from 10 to 110 mm for the D&S imaging and the SPW and LDB HFR imaging methods for the simulated data in Fig. 6. The absolute changes of the D&S imaging method are used as references and thus their relative changes are all zeros.

Table 2
Relative changes and their averages (last columns) of the −6 dB lateral beam width, ER, and SR at 6 depths of 10, 30, 50, 70, 90, and 110 mm for the HFR imaging methods based on the simulated data in Fig. 6. The relative changes of the absolute changes (see Eq. (4)) of the three parameters after adding the phase aberration and the noise are shown in Panels (a) and (b), respectively. The absolute changes of the D&S imaging method are used as references in calculating the relative changes.

	10	30	50	70	90	110	Average
(a) Add phase aberration							
SPW_width	−0.2816	−0.0039	−0.0919	−0.0216	−0.0673	−0.1522	−0.1031
SPW_ER	0.1541	−1.1024	−0.0457	0.0127	−0.0172	−0.0472	−0.1743
SPW_SR	−0.2029	−0.2233	−0.0367	0.0066	−0.0345	−0.0854	−0.0960
LDB_width	−0.2629	−0.0021	−0.1181	−0.0063	−0.0495	−0.1402	−0.0965
LDB_ER	0.3659	−1.0466	0.0049	0.0500	0.0239	−0.0113	−0.1022
LDB_SR	−0.1429	−0.1858	0.0247	0.0693	0.0526	0.0219	−0.0267
(b) Add noise							
SPW_width	−0.0060	−0.0054	−0.0523	−0.0034	−0.0221	0.0023	−0.0145
SPW_ER	−0.0469	−0.0230	−0.0159	−0.0029	−0.0018	−0.0013	−0.0153
SPW_SR	−0.0059	−0.0016	0.0027	−0.0025	−0.0142	−3.4500e−04	−0.0036
LDB_width	−0.0067	−0.0021	−0.0462	−0.0028	0.0059	0.0203	−0.0053
LDB_ER	−0.0462	−0.0223	−0.0129	−1.6000e−04	7.6000e−05	5.9300e−04	−0.0135
LDB_SR	−0.0051	0.0071	−0.0040	−0.0078	−0.0134	0.0050	−0.0030

calculated with Eq. (3) and the results are given in Table 1a. A negative value in the table means that the corresponding lateral resolution of the HFR imaging methods is higher than that of the D&S imaging method.

$$beamwidth\_diff = beamwidth\_HFR - beamwidth\_D\&S, \quad (3)$$

where *beamwidth_HFR* and *beamwidth_D&S* are the −6-dB lateral beam widths of the HFR and the D&S imaging methods respectively.

Table 1a illustrates that when there is no phase aberration or noise, the differences of −6-dB lateral resolution calculated by Eq. (3) are negative at almost of the depths. There are exceptions at the depths of 70 mm (0.1315 mm for SPW and 0.0742 mm for LDB) and at 90 mm (0.0477 mm for SPW). This is because 70 mm is the focal depth of the D&S imaging method and thus the highest resolution is achieved at this and nearby depths. The ER and SR in Fig. 6b and c are obtained without phase aberration and noise, which only have small variations over the depth.

Comparing the results of the 2nd columns with the 1st column in Fig. 6, it is clear that the −6-dB lateral resolution, ER, and SR become worse due to the phase aberration. After adding the noise, the results shown in the 3rd column of Fig. 6 also become worse.

Due to the phase aberration and the noise, there are changes of the three parameters as they are compared to those without the phase aberration and the noise. To assess whether the HFR imaging methods are more resistant to the phase aberration and the noise than the D&S imaging method, the following formula is used to calculate the changes (*relative_change*) relative to the changes (*change_for_D&S*) of the D&S method for the changes (*change*) of an imaging method for the three parameters:

$$relative\_change = |change| - |change\_for\_D\&S|, \quad (4)$$

where *change* and *change_for_D&S* are the differences of parameters after and before the addition of the phase aberration or the noise for an imaging method and the D&S imaging method, respectively. The relative changes of the −6-dB lateral beam width, ER, and SR after adding the phase aberration and the noise for the point scatterers along the axial direction are shown in Fig. 7. Apparently, if *change = change_for_D&S*, *relative_change* ≡ 0. This produces horizontal lines at value of 0 in Fig. 7.

The relative changes and their averages for the three parameters over all depths are given in Table 2. From both Table 2 and Fig. 7, it is clear that most of the relative changes are negative

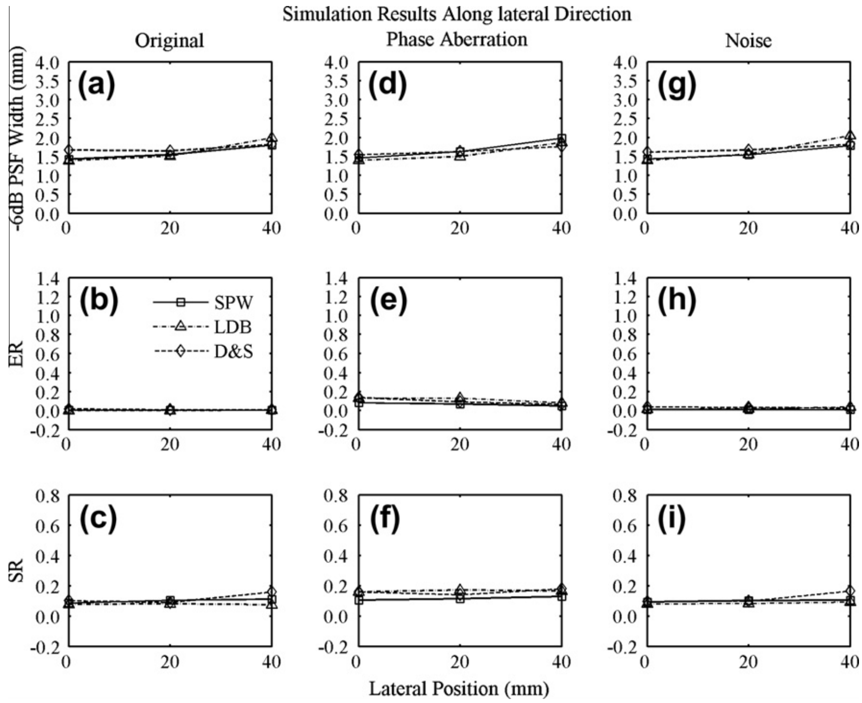

Fig. 8. This figure is the same as Fig. 6 except that it is for the three point scatterers located at lateral distances of 0, 20, and 40 mm at a depth of 50 mm.

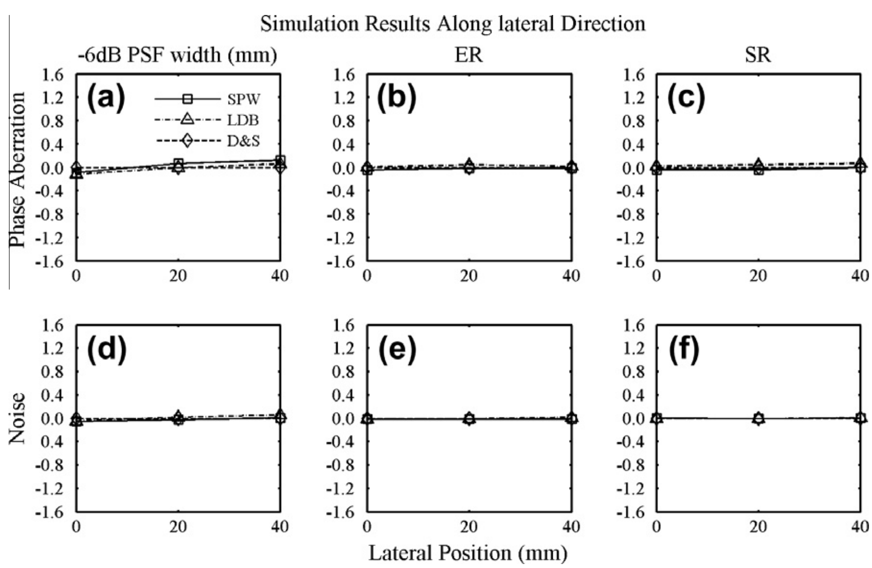

Fig. 9. This figure is the same as Fig. 7 except that it is for the three point scatterers located at lateral distances of 0, 20, and 40 mm at a depth of 50 mm.

and the averages of the relative changes are all negative. This demonstrates that the HFR imaging methods are less susceptible to the phase aberration and the noise than the D&S imaging method. In addition, the noise has less influence on the quality of images than the phase aberration (see Table 2b).

3.2.2. Simulation results for point scatterers along lateral direction

The results of the −6-dB lateral resolution, ER, and SR for point scatterers along the lateral direction at a depth of 50 mm and lateral positions of 0, 20, and 40 mm are given in Fig. 8. Comparing the 2nd and 3rd columns with the 1st on corresponding rows, it is clear that the quality of image becomes worse as either the phase aberration or the noise is introduced. Table 1b shows the differences of the −6-dB lateral beam widths relative to that of the D&S imaging method (Eq. (3)) for the plots in Fig. 8a. Values (0.1701 mm for LDB and −0.0244 mm for SPW) in the Table 1b are only positive or close to 0 for the point scatterer at 40 mm lateral distance that is near the edge. This is because fewer images are superposed near the edge of the image for the HFR imaging methods [3].

The relative changes of the −6-dB lateral beam width, ER, and SR after adding the phase aberration and after adding the noise for the point scatterers along the lateral direction are shown in Fig. 9. The average relative changes for the three parameters over the three lateral positions at 0, 20, and 40 mm are given in Table 3. From Table 3, it is seen that the average relative changes over the three lateral positions has a maximum absolute value of 0.0454. This means that the overall effects of the phase aberration and the noise in the lateral direction are not as much as those for the point scatterers in the axial direction.

4. Experiment and results

4.1. Experiment conditions

To evaluate the performance of the imaging methods for data acquired from an actual imaging system, an experiment was conducted. In the experiment, a modified AIUM 100-mm standard test object was used. A homemade HFR imaging system was used to acquire radio-frequency (RF) echo data. Details on the development and the capability of the imaging system are given in [10,11]. To be consistent with the simulation, 4 nylon wires have been added to the standard AIUM 100-mm standard test object as shown in Fig. 10. In the imaging area, there is a group of 6 point scatterers clustered together near the lower right corner of the sector area. However, these pointer scatterers are excluded from analyses because they are not assumed in the simulation. In the experiment, an Acuson V2 probe that is a 1D phased array transducer having 128 elements and 2.5-MHz center frequency was used. As mentioned before, these and other parameters in the experiment are the same as those assumed in the simulation.

Table 3
This table is the same as Table 2 except that it is for the three point scatterers located at lateral distances of 0, 20, and 40 mm at a depth of 50 mm.

	0	20	40	Average
(a) Add phase aberration				
SPW_width	−0.0919	0.0659	0.1247	0.0329
SPW_ER	−0.0457	−0.0174	−0.0136	−0.0256
SPW_SR	−0.0367	−0.0380	−0.0025	−0.0257
LDB_width	−0.1181	−0.0059	0.0607	−0.0211
LDB_ER	0.0049	0.0454	0.0190	0.0231
LDB_SR	0.0247	0.0413	0.0702	0.0454
(b) Add noise				
SPW_width	−0.0523	−0.0234	0.0082	−0.0225
SPW_ER	−0.0159	−0.0167	−0.0118	−0.0148
SPW_SR	0.0027	−0.0065	5.2000e−05	−0.0012
LDB_width	−0.0462	0.0209	0.0590	0.0112
LDB_ER	−0.0129	−0.0075	0.0169	−0.0012
LDB_SR	−0.0040	−0.0065	0.0117	3.9200e−04

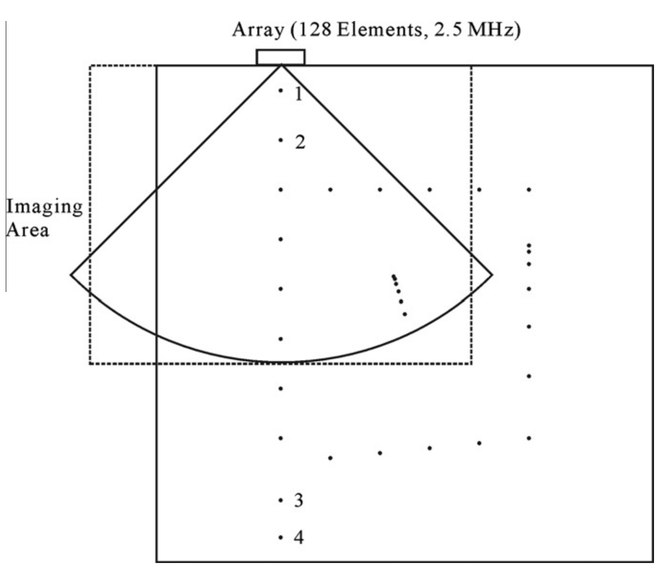

Fig. 10. A modified AIUM 100-mm test object. "1", "2", "3" and "4" are 4 nylon wires added to the standard AIUM 100-mm test object, but only "1" (at the depth of 10 mm) and "2" (at the depth of 30 mm) are within the imaging area for the experiment in this paper. 6 point scatterers in the axial direction are located at depths of 10, 30, 50, 70, 90, and 110 mm, respectively, and 2 point scatterers in the lateral direction are located at lateral positions of 20 and 40 mm, respectively. Point scatterers that are clustered near the bottom-right corner of the fan-shaped area are not used in the study since they are not assumed in the simulation. The dashed rectangle gives an area of final B-mode images, which has a size of 153.6 mm in width and 120 mm in depth.

4.2. Experiment results

Images obtained from the experiment without adding the phase aberration and the noise, after adding the phase aberration, and after adding the pseudo-random noise are shown in Fig. 11. It is clear that the image quality is decreased due to the addition of the phase aberration and the noise. The three parameters, the −6-dB lateral beam width, ER, and SR are calculated for all images in Fig. 11 and the results for point scatterers along the axial and lateral directions are shown in Figs. 12 and 14, respectively.

4.2.1. Experiment results for point scatterers along axial direction

Comparing Figs. 12a with 6a, it is seen that the −6-dB lateral beam width at the depth of 10 mm is around 2.5 mm, which is much larger than 0.4 mm at the same depth in the simulation. This is due to the leaking of transmit pulses into the receiver amplifier at the beginning of data acquisition. As is in the simulation, the differences of the −6-dB lateral beam widths between the HFR and the D&S imaging methods can be calculated with Eq. (3) (see Table 4a). The all-negative values in this table indicate that the resolution of the HFR imaging methods is higher than that of the D&S imaging method. This is different from the simulation and may be caused by multiple factors that may not be considered in the simulation. Without the phase aberration and the noise, ER and SR have only relatively small variations over the depth (see Fig. 12b and c), which is similar to those in the simulation. Again, after adding the phase aberration and the noise, ER and SR increase significantly.

The relative changes (see Eq. (4) above) of the −6-dB lateral beam width, ER, and SR of the images of point scatterers along the axial direction are shown in Fig. 13. The relative changes of ER after adding the phase aberration or the noise for point scatterers close to the surface of the transducer are much smaller for the HFR imaging methods than for the D&S imaging method (see Fig. 13b and e). This is because there are more sub-images superposed coherently near the surface of the transducer to reduce the effects of the phase aberration or the noise (it is superposed close to 91 times due to 91 transmissions).

The relative changes and their averages of the three parameters for the point scatterers over the 6 depths are listed in Table 5. The averages of the relative changes are almost all negative in all cases. This demonstrates that the changes caused by the phase aberration or the noise for the HFR imaging methods are smaller than those for the D&S imaging method. In other words, the HFR imaging methods are more resistant to the phase aberration and the noise than the D&S method.

4.2.2. Experiment results for point scatterers along lateral direction

The −6-dB lateral beam width, ER, and SR of the images of the point scatterers at the depth of 50 mm and at lateral positions of 0, 20, and 40 mm in Fig. 11 are given in Fig. 14. The differences of the −6-dB beam widths between the HFR and the D&S imaging methods are calculated from Fig. 14a with Eq. (3) and are shown in Table 4b. The all-negative values means that the HFR imaging methods have a higher lateral resolution than the D&S imaging method at all lateral positions. In addition, the ER and SR values for the D&S imaging method are also generally larger than those of the HFR imaging methods (see the 2nd and the 3rd rows of Fig. 14).

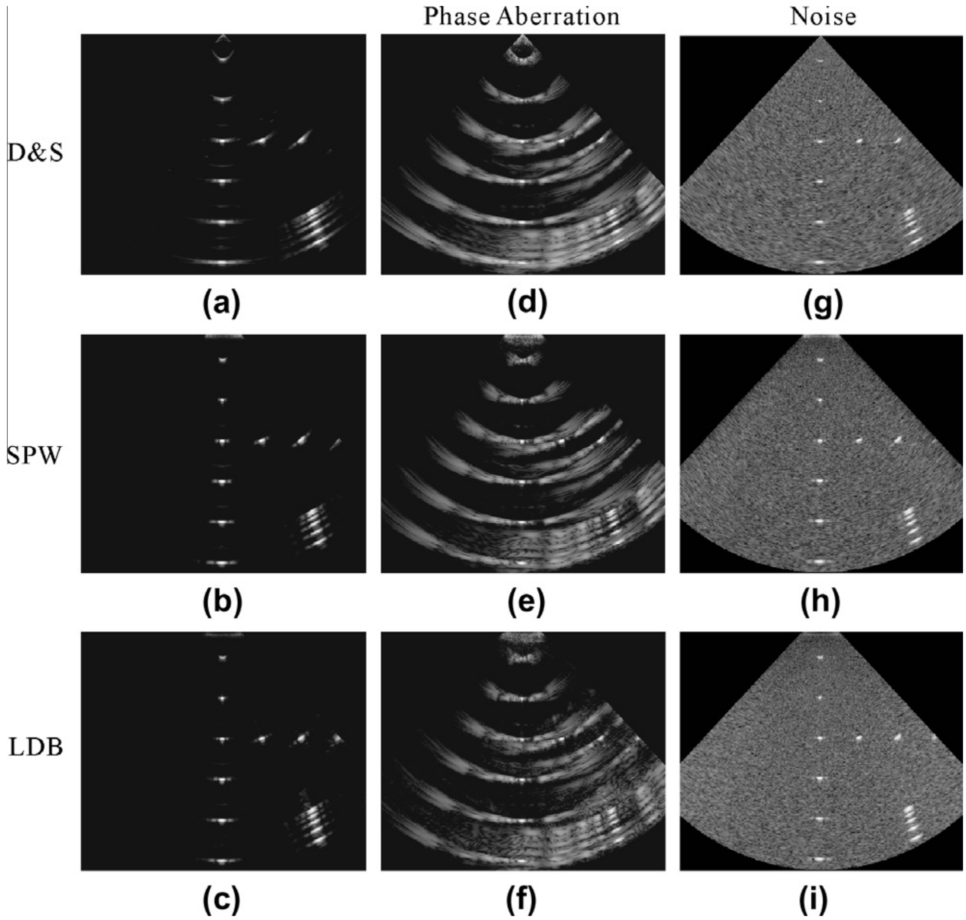

Fig. 11. This figure is the same as Fig. 5 except that it is obtained with experiment data.

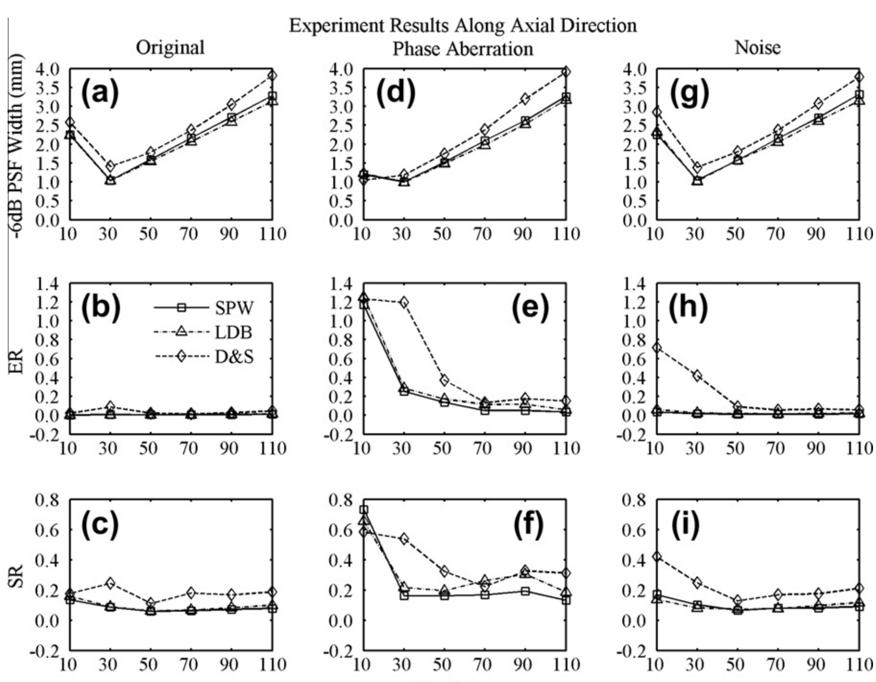

Fig. 12. This figure is the same as Fig. 6 except that it is obtained with experiment data.

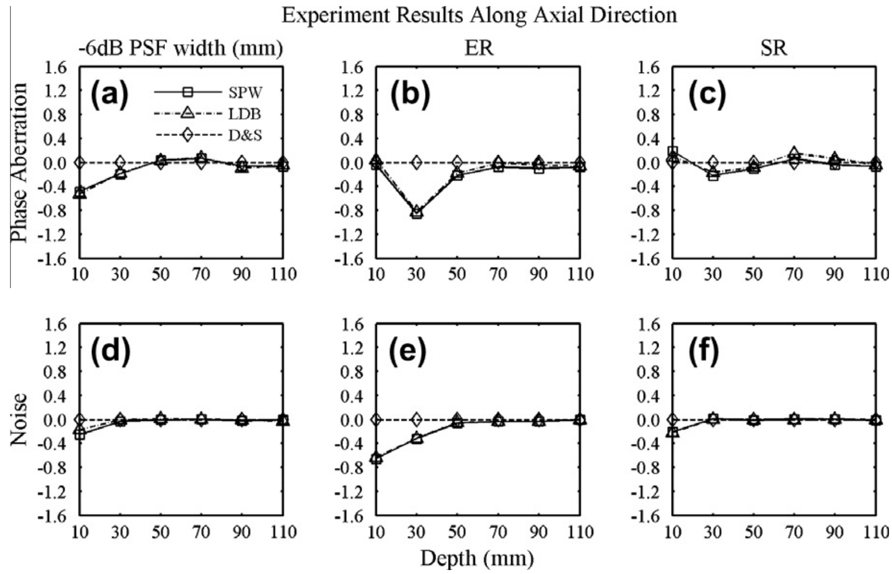

Fig. 13. This figure is the same as Fig. 7 except that it is obtained with experiment data.

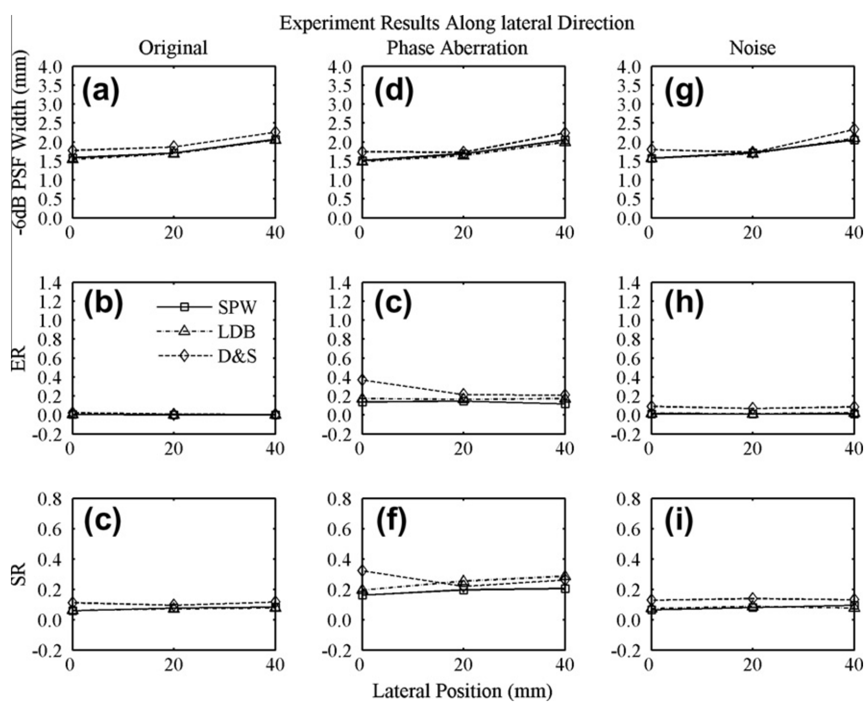

Fig. 14. This figure is the same as Fig. 8 except that it is obtained with experiment data.

Table 4
This table is the same as Table 1 except that it is obtained with experiment data.

	10	30	50	70	90	110
(a)						
SPW	−0.3342	−0.3701	−0.1953	−0.2069	−0.3356	−0.5376
LDB	−0.3460	−0.3736	−0.2344	−0.3103	−0.4584	−0.6889
		0		20		40
(b)						
SPW		−0.1953		−0.1568		−0.1915
LDB		−0.2344		−0.1800		−0.2022

Fig. 15 shows the relative changes of the −6-dB lateral beam width, ER, and SR for point scatterers along the lateral direction after the addition of the phase aberration and the noise. The relative changes and their averages of the three parameters for the point scatterers at 0, 20, and 40 mm are given in Table 6. The average relative changes in the table are almost all negative, indicating that the HFR imaging methods are more resistant to the phase aberration and the noise.

5. Discussion

From the results of the simulation and the experiment in Sections 3 and 4, it is clear that the set of parameters, i.e., the −6-dB lateral resolution, ER, and SR can be used to quantitatively assess the effects of phase aberration and pseudo-random noise on

Table 5
This table is the same as Table 2 except that it is obtained with experiment data.

	10	30	50	70	90	110	Average
(a) Add phase aberration							
SPW_width	−0.4855	−0.1940	0.0350	0.0660	−0.0624	−0.0680	−0.1181
SPW_ER	−0.0418	−0.8590	−0.2132	−0.0747	−0.1047	−0.0795	−0.2288
SPW_SR	0.1911	−0.2195	−0.1091	0.0620	−0.0393	−0.0706	−0.0309
LDB_width	−0.5264	−0.1807	0.0305	0.0808	−0.0917	−0.0397	−0.1212
LDB_ER	0.0420	−0.8243	−0.1814	−0.0120	−0.0440	−0.0615	−0.1802
LDB_SR	0.0899	−0.1662	−0.0786	0.1517	0.0617	−0.0380	0.0034
(b) Add noise							
SPW_width	−0.2534	−0.0300	−0.0065	0.0037	−0.0186	−0.0081	−0.0521
SPW_ER	−0.6628	−0.3203	−0.0596	−0.0338	−0.0359	−0.0056	−0.1863
SPW_SR	−0.2079	0.0117	−0.0106	0.0050	0.0022	−0.0122	−0.0353
LDB_width	−0.1701	−0.0081	0.0099	0.0025	−0.0066	−0.0317	−0.0340
LDB_ER	−0.6356	−0.3144	−0.0540	−0.0340	−0.0331	−0.0066	−0.1796
LDB_SR	−0.2241	0.0036	−0.0041	−0.0017	0.0062	−0.0062	−0.0377

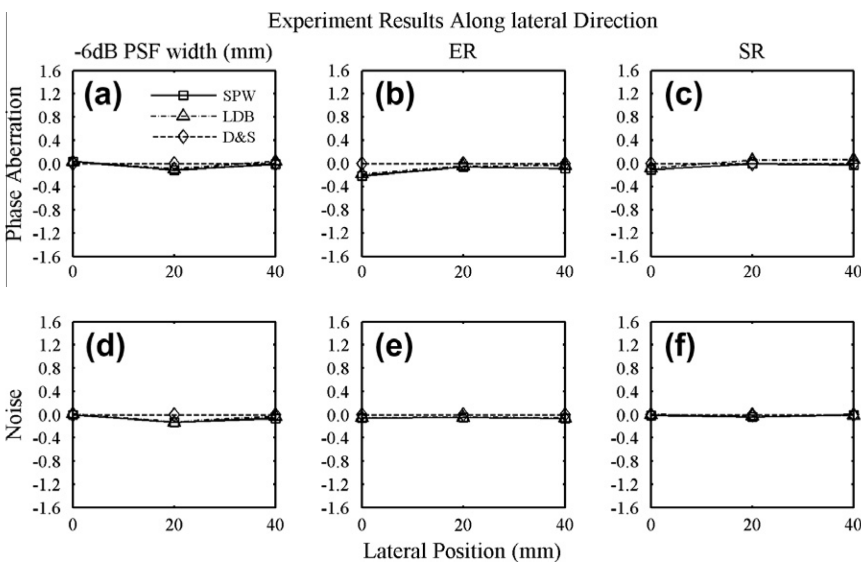

Fig. 15. This figure is the same as Fig. 9 except that it is obtained with experiment data.

Table 6
This table is the same as Table 3 except that it is obtained with experiment data.

	0	20	40	Average
(a) Add phase aberration				
SPW_width	0.0350	−0.1166	−0.0106	−0.0307
SPW_ER	−0.2132	−0.0617	−0.0907	−0.1219
SPW_SR	−0.1091	−0.0046	−0.0235	−0.0457
LDB_width	0.0305	−0.0932	0.0389	−0.0079
LDB_ER	−0.1814	−0.0415	−0.0341	−0.0857
LDB_SR	−0.0786	0.0585	0.0654	0.0151
(b) Add noise				
SPW_width	−0.0065	−0.1329	−0.0663	−0.0685
SPW_ER	−0.0596	−0.0515	−0.0695	−0.0602
SPW_SR	−0.0106	−0.0415	−0.0033	−0.0185
LDB_width	0.0099	−0.1311	−0.0297	−0.0503
LDB_ER	−0.0540	−0.0485	−0.0582	−0.0536
LDB_SR	−0.0041	−0.0272	−0.0152	−0.0155

imaging methods. From Table 4, it is clear that in the experiment, the HFR imaging methods have higher −6-dB lateral resolutions at all depths and all lateral positions than the D&S imaging method. The average differences of the −6-dB lateral beam widths as compared to the D&S imaging method over all the imaging depths and lateral positions are −0.1337 mm for SPW and −0.1481 mm for LDB in simulation. In experimentation, the average differences are −0.2804 mm for SPW and −0.3365 mm for LDB. According to the inverse relationship between image resolution and beam width, the negative values show that the HFR imaging method outperforms the D&S imaging method in terms of the imaging resolution.

The results in Figs. 7 (simulation) and 13 (experiment) show that the image quality of point scatterers near the surface of the transducer is more susceptible to phase aberration and noise than at deeper depths. In general, curves of the HFR imaging methods in Figs. 7 and 13 are smaller than zero. This means that the HFR imaging methods are affected less by the phase aberration and the noise than the D&S imaging method. This is also supported by Tables 2 and 5 where the average relative changes have mostly negative values. As for the results from the lateral direction (see Figs. 9 and 15, and Tables 3 and 6), the experiment produced mostly negative average relative change values. This means that the experiment also demonstrates that the HFR imaging methods are less susceptible to the phase aberration and the noise than the D&S imaging method.

In the simulation study of phase aberration, the average relative changes over all the imaging depths and lateral positions of the −6-dB lateral beam width, ER, and SR are −0.0351, −0.1000, and −0.0609, respectively, for SPW; and -0.0588, -0.0396, and 0.0187, respectively, for LDB. In the experimentation, the average relative changes of the three parameters corresponding to the simulation are −0.0744, −0.1754, and −0.0383, respectively, for SPW; and −0.06455, -0.1330, and 0.0093, respectively, for LDB. The negative values indicate that the HFR imaging method is less affected by the phase aberration than the D&S imaging method. The small positive values, 0.0187 and 0.0093, are due to the point scatterer at the edge of the imaging area, where there is less superposition for the HFR imaging method.

As for the studies of the effects of the noise, the simulation results show that the average relative changes of the −6-dB lateral beam width, ER, and SR are −0.0185, −0.0151, and −0.0024, respectively, for SPW; and 0.0030, −0.0074, and −0.0013, respectively, for LDB. In the experiment, the average relative changes of the −6-dB lateral beam width, ER, and SR caused by the noise are −0.0603, −0.1233, and −0.0269, respectively, for SPW; and −0.0422 to 0.1166, and −0.0266, respectively, for LDB. The mostly negative values also indicate that the HFR imaging method is less influenced by the noise than the D&S imaging method.

6. Conclusion

This paper uses a set of parameters to assess and compare the image quality of the HFR and the D&S imaging methods. These parameters include the traditional −6-dB lateral resolution, and the newly developed parameters ER and SR. From the study, it is found that the HFR imaging methods have a higher lateral image resolution than the D&S imaging method in the experiment and this is also true in the simulation except at the depths near the focus of the transmit beams of the D&S imaging method. The results also show that the HFR imaging methods are less affected by phase aberration and noise. These results are consistent with those obtained from previous studies. However, the studies carried out in this paper are different from the previous ones since the current studies are based on the point spread function (PSF) that is the basis of any linear imaging system. In addition, the current studies is more comprehensive since they cover a wider range of image depths from 10 to 110 mm and cover lateral positions from 0 to 40 mm at a depth of 50 mm.

The parameters, the −6-dB lateral resolution, ER, and SR, that are defined based on the PSF of imaging systems provide a simple but quantitative method to study the effects of phase aberration and noise on the HFR and D&S imaging methods. These parameters can also be used to quantitatively assess quality of images of other imaging methods.

References

[1] J.-y. Lu, 2D and 3D high frame rate imaging with limited diffraction beams, IEEE Trans. Ultrason. Ferroelectr. Freq. Control. 44 (Jul 1997) 839–856.
[2] J.-y. Lu, Experimental study of high frame rate imaging with limited diffraction beams, IEEE Trans. Ultrason. Ferroelectr. Freq. Control. 45 (Jan 1998) 84–97.
[3] J.Q. Cheng, J.-y. Lu, Extended high-frame rate imaging method with limited-diffraction beams, IEEE Trans. Ultrason. Ferroelectr. Freq. Control. 53 (May 2006) 880–899.
[4] J.-y. Lu, A study of signal-to-noise ratio of the fourier method for construction of high frame rate images, Acoust. Imaging 24 (2000) 401–405.
[5] J.-y. Lu, S.P. He, Effects of phase aberration on high frame rate imaging, Ultrasound Med. Biol. 26 (Jan 2000) 143–152.
[6] J. Wang, J.-y. Lu, Effects of phase aberration and noise on extended high frame rate imaging, Ultrason. Imaging 29 (Apr 2007) 105–121.
[7] J.F. Greenleaf, B. Rajagopalan, P.J. Thomas, S.A. Johnson, R.C. Bahn, Variation of acoustic speed with temperature in various excised human tissues studied by ultrasound computerized tomography, in: M. Linzer (Ed.),Ultrasonic Tissue Characterization II: A Collection of Reviewed Papers Based on Talks Presented at the Second International Symposium on Ultrasonic Tissue Characterization Held at the National Bureau of Standards, Gaithersburg, Maryland, June 13–15, 1977, Dept. of Commerce, National Bureau of Standards, Washington, 1979, pp. 227–233..
[8] J. Wang, J.-y. Lu, A study of motion artifacts of Fourier-based image construction, in: 2005 IEEE Ultrasonics Sympo., vols. 1–4, 2005, pp. 1439–1442.
[9] J.-y. Lu, J. Cheng, Field computation for two-dimensional array transducers with limited diffraction array beams, Ultrason. Imaging 27 (Oct 2005) 237–255.
[10] J.-y. Lu, J. Wang, Square-wave aperture weightings for reception beam forming in high frame rate imaging, in: 2006 IEEE Ultrason. Sympo., vols. 1–5, Proceedings, 2006, pp. 124–127.
[11] J.-y. Lu, J.Q. Cheng, J. Wang, High frame rate imaging system for limited diffraction array beam imaging with square-wave aperture weightings, IEEE Trans. Ultrason. Ferroelectr. Freq. Control. 53 (Oct 2006) 1796–1812.